How to cite: *Angew. Chem. Int. Ed.* **2021**, *60*, 13937–13944
International Edition: doi.org/10.1002/anie.202102082
German Edition: doi.org/10.1002/ange.202102082

Peptidomimetics Hot Paper

Bicyclic β-Sheet Mimetics that Target the Transcriptional Coactivator β-Catenin and Inhibit Wnt Signaling

*Mathias Wendt, Rosa Bellavita, Alan Gerber, Nina-Louisa Efrém, Thirza van Ramshorst, Nicholas M. Pearce, Paul R. J. Davey, Isabel Everard, Mercedes Vazquez-Chantada, Elisabetta Chiarparin, Paolo Grieco, Sven Hennig, and Tom N. Grossmann**

Abstract: *Protein complexes are defined by the three-dimensional structure of participating binding partners. Knowledge about these structures can facilitate the design of peptidomimetics which have been applied for example, as inhibitors of protein–protein interactions (PPIs). Even though β-sheets participate widely in PPIs, they have only rarely served as the basis for peptidomimetic PPI inhibitors, in particular when addressing intracellular targets. Here, we present the structure-based design of β-sheet mimetics targeting the intracellular protein β-catenin, a central component of the Wnt signaling pathway. Based on a protein binding partner of β-catenin, a macrocyclic peptide was designed and its crystal structure in complex with β-catenin obtained. Using this structure, we designed a library of bicyclic β-sheet mimetics employing a late-stage diversification strategy. Several mimetics were identified that compete with transcription factor binding to β-catenin and inhibit Wnt signaling in cells. The presented design strategy can support the development of inhibitors for other β-sheet-mediated PPIs.*

Introduction

In protein complexes, binding partners adopt defined three-dimensional structures in which amino acid (aa) side chains are aligned to facilitate intermolecular interactions. The mimicry of underlying secondary and tertiary structures has provided selective and high-affinity ligands that have been used for the elucidation and modulation of biological processes.[1] Peptidomimetic structures proved particularly useful for the inhibition of protein–protein interactions (PPIs),[2] here mainly recapitulating α-helices.[3] Even though β-sheets occur frequently in PPIs,[4] the corresponding mimetics have been less explored as PPI inhibitors.[5] In general, most β-sheet mimetics are based on β-hairpin peptides which comprise two antiparallel β-strands connected by a turn.[5b,6] The β-hairpin structure can be stabilized by backbone modifications within the β-strands, β-sheet-inducing turn mimetics and by hairpin macrocyclization.[5–7] Macrocyclization has predominantly been implemented via head-to-tail as well as cross-strand tethers with the latter using different crosslinks such as disulfides,[8] triazoles,[9] amides,[10] thioethers [10c,11] and hydrocarbon structures.[11b,12] Owing to the often low tendency of β-hairpin mimetics to penetrate cells, they have been mainly applied to target extracellular PPIs[5,8a] thereby excluding a large number of highly interesting intracellular PPIs.

The inhibition of certain pathological PPIs is considered a promising therapeutic approach for numerous diseases.[13] Due to the extended nature of involved interaction areas,[14] conventional ligand-discovery approaches that rely on small molecular scaffolds often fail to provide potent PPI inhibitors.[15] A prime example for a therapeutically interesting protein which participates in numerous PPIs is the transcriptional coactivator β-catenin serving as the central intracellular interaction hub of the Wnt signaling pathway.[16] Importantly, β-catenin binding to transcription factor proteins of the T-cell factor (TCF) family activates the expression of Wnt target genes thereby stimulating cell growth and proliferation.[17] Hyperactivation of the Wnt pathway is associated with various forms of cancer rendering the inhibition of the β-catenin/TCF interaction an attractive strategy for therapeutic intervention.[18] Due to the challenges associated with the use of small molecules,[19] the development of peptide-derived PPI inhibitors has been pursued.[20] However, these efforts have not resulted in therapeutically useful inhibitors of the β-catenin/TCF interaction mainly due to their unfavorable physico-chemical properties and/or low bioavailability.[19] The development of inhibitors would greatly benefit from novel

[*] M. Wendt, R. Bellavita, A. Gerber, N.-L. Efrém, T. van Ramshorst, N. M. Pearce, S. Hennig, T. N. Grossmann
Department of Chemistry and Pharmaceutical Sciences
VU University Amsterdam
Amsterdam (The Netherlands)
E-mail: t.n.grossmann@vu.nl
R. Bellavita, P. Grieco
Department of Pharmacy, University of Naples Federico II
Naples (Italy)
P. R. J. Davey, E. Chiarparin
Medicinal Chemistry, Oncology R&D, AstraZeneca
Cambridge (UK)
I. Everard, M. Vazquez-Chantada
Mechanistic Biology and Profiling, Discovery Sciences, R&D, AstraZeneca
Cambridge (UK)
Supporting information and the ORCID identification number(s) for the author(s) of this article can be found under: https://doi.org/10.1002/anie.202102082.

cell-permeable and high affinity ligands ideally with a structurally characterized binding mode to support subsequent optimization efforts towards clinical inhibitors.

Here, we describe the structure-based design of β-sheet mimicking bicycles that target β-catenin and inhibit its interaction with a TCF transcription factor. Based on the known structure of β-catenin in complex with the protein E-cadherin, a macrocyclic binder of β-catenin was developed which comprises a short antiparallel β-sheet. A crystal structure of the macrocycle bound to β-catenin was obtained supporting the design of a library of bicyclic peptidomimetics. Among those mimetics, we identified a bicycle (**A-b6**) that inhibits the Wnt signaling pathway in a cell-based assay and shows cellular uptake comparable to the cell penetrating **Tat** peptide.

Results and Discussion

E-Cadherin-Derived Peptides Bind β-Catenin

β-Catenin consists of 781 amino acids and comprises a central armadillo repeat domain (aa 141–664), which is flanked by flexible N- and C-terminal regions. The armadillo repeats serve as interaction hub recognizing several protein binding partners.[19a] The family of TCF transcription factors is among those binders and shares homologous β-catenin binding domains (CBDs) that bind a central region of the armadillo repeat domain.[21] These CBDs usually encompass an α-helix and an extended sequence which are connected via a flexible loop (CBD of TCF-4, green, Figure 1a). The extended region includes a short β-strand with two crucial hot-spot amino acids (D16 and E17 in TCF-4)[22] that bind β-catenin on the so-called "binding site 3".[19a]

Herein, we aimed to design a ligand capable of targeting β-catenin's binding site 3 to compete with TCF binding. When inspecting available β-catenin complex structures, we noticed that the CBD of E-cadherin (orange, Figure 1a), a protein that recruits β-catenin to cell-cell adhesions junctions, includes a small antiparallel β-sheet which also binds to β-catenin's binding site 3. Initially, we considered a 52 aa sequence (**E-CBD**, aa 628–679, Figure 1a) that encompasses an α-helix (α1, aa 652–665) and the two antiparallel β-strands (β1: aa 628–633; β2: aa 674–679) including intervening loop regions. Notably, two of the five predicted hot-spots of **E-CBD** (D674 and L676)[23] are located within strand β2 (Figure 1a). A fluorescently labeled version of **E-CBD** was synthesized with the one methionine (M638) present substituted by the chemically inert analogue norleucine. A fluorescence polarization (FP) assay applying full length β-catenin revealed a high binding affinity for **E-CBD** (dissociation constant (K_d) = 0.053 μM). Keeping β2 as the anchor point, a series of N-terminally truncated and labeled **E-CBD** versions was synthesized (Figure 1b). While the deletion of 7 or 13 amino acids (peptides **1** and **2**) only moderately affected affinity for β-catenin (K_d = 0.13 and 0.2 μM, respectively), a truncation to 28-mer **3** severely reduced binding (K_d approx. 3 μM).

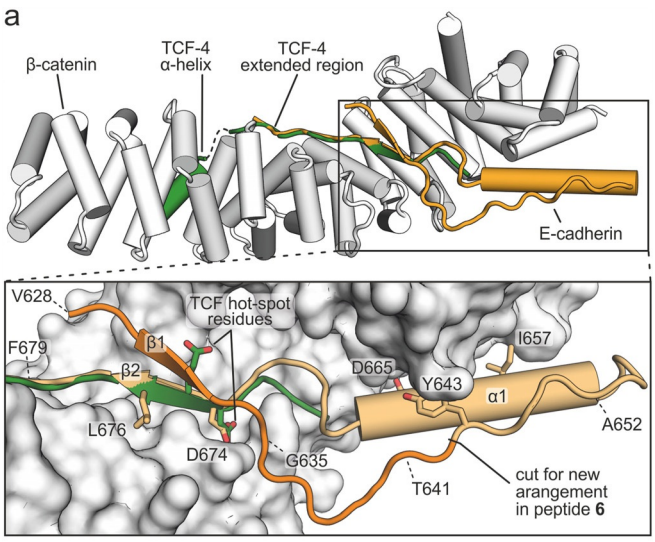

b

Peptide	K_d / μM	length
E-CBD	0.053 ±0.003	52 aa
1	0.13 ±0.04	45 aa
2	0.2 ±0.1	39 aa
3	~ 3	28 aa

c

Peptide	K_d / μM	length
6	0.18 ±0.03	54 aa
8	0.053 ±0.005	48 aa
9	>5	23 aa
10	0.6 ±0.1	45 aa
11	>5	14 aa

Figure 1. a) Top: Crystal structure (PDB ID 2gl7) of β-catenin (grey) in complex with the CBD of TCF-4 (green) and superimposed with the CBD of E-cadherin (orange, PDB ID 1i7x, chain B). Bottom: Close-up of indicated region with β-catenin in surface representation (grey). Hot-spot amino acids of **E-CBD** (D665, I657, Y643, D674, L676) and TCF (D16, E17) are shown as stick. Terminal amino acids of peptides **E-CBD**, **1**, **2** and **3** are indicated. Position where sequence of **E-CBD** was opened to generate peptide **6** is indicated (for details see Supporting Figure S2). b) Peptide affinities and lengths are shown including the visualization of involved peptide regions. K_d-values were obtained from FP measurements (n = 3, ± std. error, for binding curves see Supporting Figure S1). c) Table shows peptides derived from **6**. The β-alanine loop (βA-βA) is highlighted in black. Measurements in analogy to Figure 1b. Peptide sequences can be found in Supporting Table S1.

Seeking a short peptide sequence suitable for subsequent stabilization via chemical modification, we aimed to place strand β2 in the center of the primary peptide sequence, thereby facilitating an alternative truncation pattern. For that purpose, we took advantage of the spatial proximity of the C- and N-terminus in **E-CBD** (F679 and V628, respectively, d = 6.5 Å, Figure 1a), which we aimed to covalently link. In this alternative arrangement, the new peptide termini were generated by opening the sequence between Y643 (new N-terminus) and Q642 (new C-terminus, Figure 1a). Between V628 and F679, different linker structures were considered

(Supporting Figure S2). The D-proline-L-proline (DP-LP)[6,24] motif was introduced in combination with an additional glycine (peptide **4**) or β-alanine (peptide **5**) to align the two termini. Both peptides exhibited low affinities for β-catenin (in both cases: K_d approx. 2 μM). The incorporation of two β-alanines yielded peptide **6** with only mildly reduced affinity ($K_d = 0.18$ μM) when compared to **E-CBD** ($K_d = 0.053$ μM). The introduction of three β-alanine residues (peptide **7**) resulted in a lower affinity ($K_d = 0.38$ μM). Using peptide **6** as a starting point, a series of truncated peptides was synthesized (Figure 1c). While the deletion of the N-terminal loop (6 aa) was tolerated (peptide **8**, $K_d = 0.053$ μM), helix α1 appeared to be essential for binding (peptide **9**, $K_d > 5$ μM). On the C-terminus, the deletion of the loop (9 aa) moderately reduced binding (peptide **10**, $K_d = 0.6$ μM). As expected, the combination of the truncations of **9** and **10** resulted in a peptide with very low affinity (peptide **11**, $K_d > 5$ μM). These truncation studies indicate that linear versions of the E-cadherin CBD require about 40 aa for sub-micromolar binding affinities.

A Cyclic Peptide Inhibits the β-Catenin/TCF-4 Interaction

Seeking a smaller binder that includes strand β2 and would therefore target β-catenin's binding site 3 (Figure 1a), we considered macrocyclization of peptide **11**. When assuming a binding mode analogous to the CBD of E-cadherin, the termini of peptide **11** would be in proximity (V633 and D674, $d = 5.2$ Å, Supporting Figure S3). Aiming for the stabilization of the antiparallel β-sheet, the DP-LP turn mimetic[6,24] was incorporated to provide macrocycle **12** (Figure 2a). Initially, a linear precursor (H_2N-βA-VTRNDV-DP-LP-DSLLVF-βA-OH) of **12** was synthesized on solid-support using 2-chlorotrityl chloride resin. After cleavage, the side-chain-protected peptide was head-to-tail cyclized in solution. Then all protecting groups were removed, and after purification, macrocycle **12** was obtained in overall yields of about 10% (Supporting Figure S4). To evaluate the binding of **12**, a competition FP assay was performed. Briefly, full-length β-catenin and a fluorescently labeled TCF-4-derived tracer peptide[20f] (Supporting Figure S5) were incubated with varying concentrations of competitor to provide half-maximal

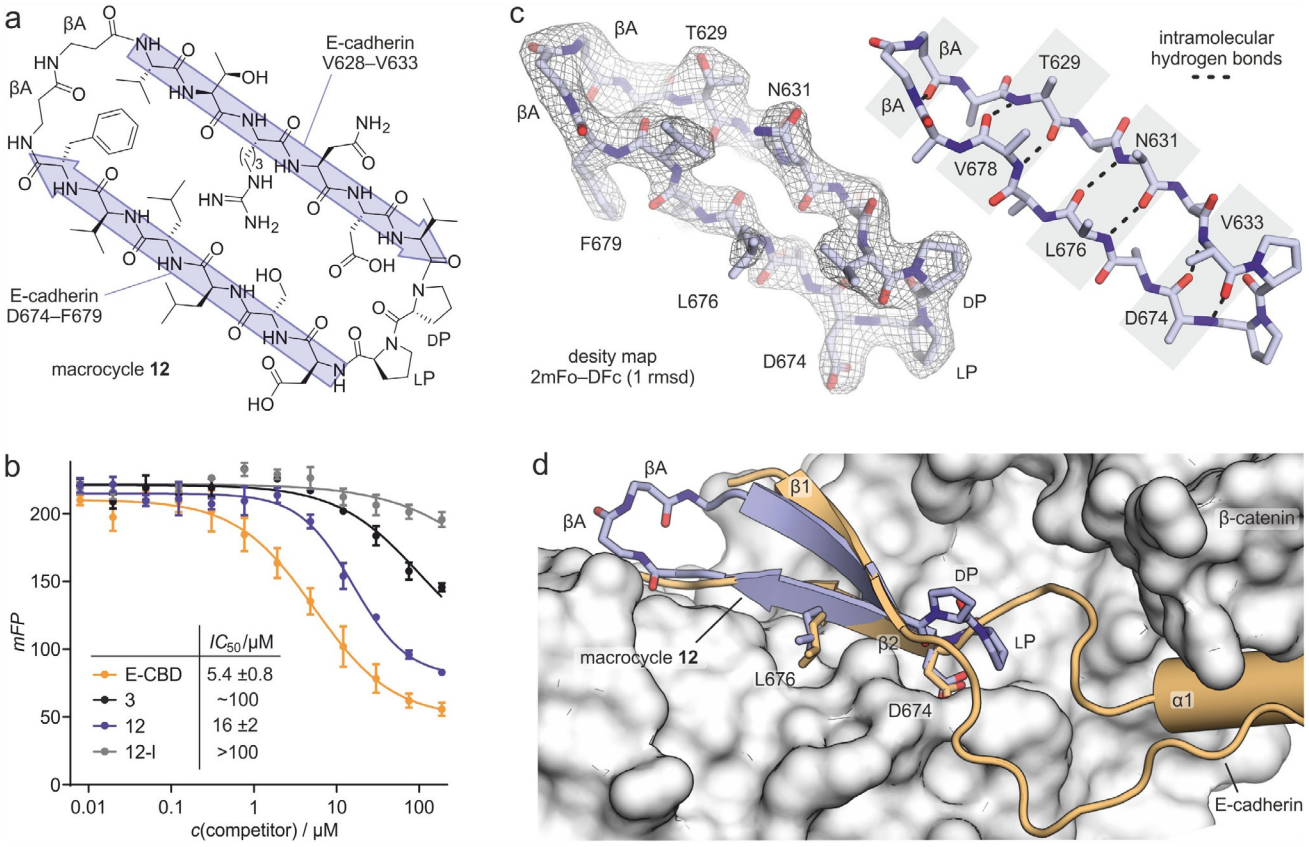

Figure 2. a) Chemical structure of the macrocycle **12**. Amino acids of β-strands β1 and β2 are highlighted in blue. b) FP competition assay with TCF-4-derived tracer peptide ($c = 10$ nM) and full-length β-catenin ($c = 250$ nM, Supporting Figure S5). Competitor concentration was varied ($c = 7.9 \times 10^{-3}$–188 μM, $n = 3$, ± std. error). Peptide sequences can be found in the Supporting Tables S1 and S2. c) Left: Electron density map (2mFo-DFc, contoured at 1 rmsd) of cyclic peptide inhibitor **12** (PDB ID 7ar4). Right: Stick representation of peptide **12** when bound to β-catenin, showing backbone atoms and C_β-atoms (PDB ID 7ar4). Intramolecular hydrogen bonds are indicated with dashed lines. d) Crystal structure of β-catenin (grey, surface representation) in complex with peptide **12** (blue, cartoon representation, PDB ID 7ar4). The hot spot residues as well as βA-βA and the DP-LP turn are shown in stick representation (blue). **12** is superimposed with the CBD of E-cadherin (orange, cartoon representation, PDB ID 1i7x). Residues L676 and D674 are shown explicitly. Data collection and refinement statistics for the PDB ID 7ar4 can be found in Supporting Table S3 (βA: β-alanine).

inhibitory concentrations (IC_{50}, Figure 2b). In this assay, macrocycle **12** showed good inhibition ($IC_{50} = 16$ μM), being only threefold less potent than the 52-mer peptide **E-CBD** ($IC_{50} = 5.4$ μM). In comparison, linear 28-mer peptide **3** (IC_{50} approx. 100 μM) and a linear version of **12** lacking the β-alanine linker (peptide **12-l**, $IC_{50} > 100$ μM) showed greatly diminished competition.

To investigate the binding mode of peptide **12**, co-crystallization with the armadillo repeat domain of β-catenin (aa 134–665) was pursued. After obtaining crystallization conditions from initial screening, crystals were optimized and analyzed by X-ray diffraction. We collected a dataset and included reflections up to 2.6 Å resolution. The structure was solved in space group $P2_12_12_1$ (PDB ID 7ar4, Supporting Table S3) using molecular replacement with β-catenin as the search model (derived from PDB ID 1jdh). The obtained crystal structure shows one copy of the β-catenin armadillo repeat domain per asymmetric unit (Supporting Figure S6). Except for one loop (aa 550–559), protein residues are well-resolved and superimpose closely with previously reported structures (PDB ID 1jdh and 2gl7, Supporting Figure S7). At β-catenin's binding site 3, additional well-defined electron density was observed matching the molecular structure of macrocycle **12** (Figure 2c, Supporting Figure S6). In complex with β-catenin, **12** closely resembles the conformation of the two antiparallel strands β1 and β2 of E-cadherin (Figure 2d, for Ramachandran plot of **12** see Supporting Figure S8). The β-hairpin in **12** is stabilized by six intramolecular hydrogen bonds within the β-sheet (two between each of the following aa pairs: T629/V678, N631/L676 and V633/D674, Figure 2c) and one additional hydrogen bond within the β-alanine turn contributing to the stabilization of the hairpin structure. The crystal structure also revealed that the predicted **E-CBD** hot spot residues (L676, D674) closely overlay with the corresponding side chains in macrocycle **12** which form analogous contacts with β-catenin. Consequently, the binding site of **12** overlaps also with the hot-spot region of TCF (Figure 1a, Supporting Figure S9) which is in line with the observed inhibition of TCF-4 binding (Figure 2b).

Bicyclization of β-Hairpin Structures

Utilizing the structure of macrocycle **12** in complex with β-catenin, the design of more constrained β-hairpin structures was pursued. We aimed for the introduction of a cross-strand bridge and identified three potentially suitable amino acid pairs located in the core of the β-hairpin (A: T629/V678, B: N631/L676, C: D632/S675, Figure 3a). To allow the installation of different bridges at a late stage of the synthesis, we decided to introduce two cysteines which, after the initial head-to-tail cyclization, are reacted with a bis-electrophile (Figure 3b). This crosslinking chemistry proved already useful for the cyclization of α-helices and loop structures.[25] A small library of bis-electrophiles (**e1**–**e7**, Supporting Figure S10) was assembled resulting in bridge structures that ranged from one to four bridging atoms between the cysteines (b1–b7, Figure 3c). Bridge b1, b2, b3 and b5 are fully saturated, while b4 and b6 include a double bond. Bridge b7

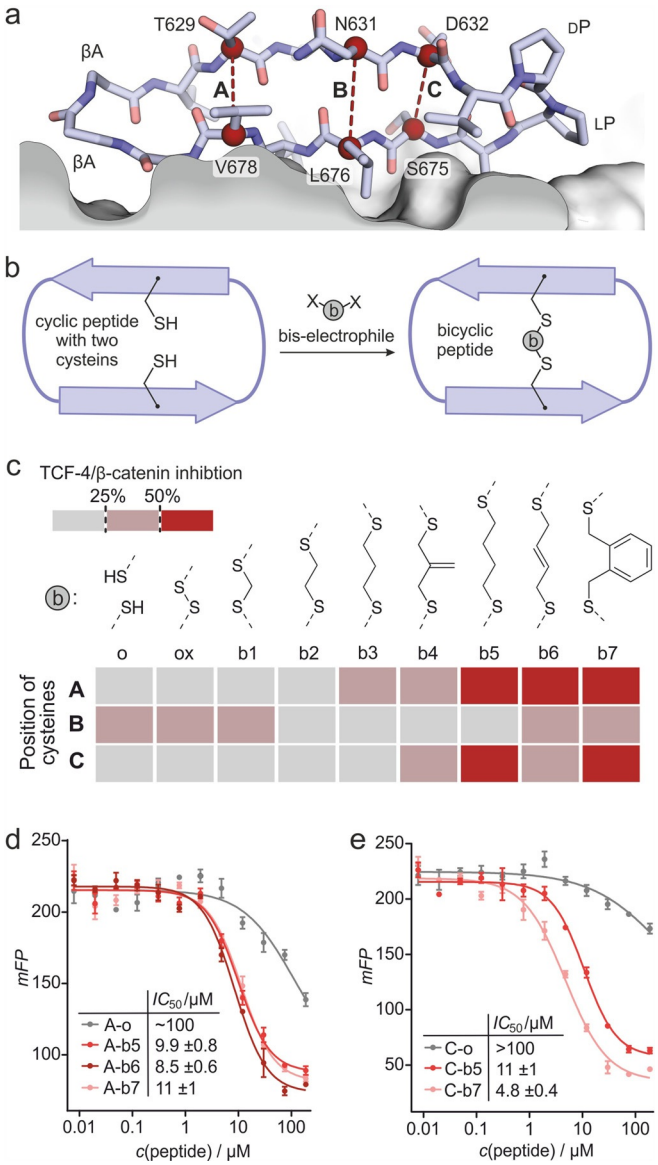

Figure 3. a) Crystal structure of **12** (blue) bound to β-catenin (grey, PDB ID 7ar4) highlighting positions in **12** selected for cross-strand bridges (A–C). C_α-atoms of the corresponding amino acids are shown as red sphere. b) Bicyclization of monocyclic **12** derivatives bearing two cysteines at cross-strand positions. Crosslinking with bis-electrophiles (**e1**–**e7**, Supporting Figure S10). Bicycle sequences can be found in Supporting Table S2. c) Chemical structures of bridges b1–7, which have been introduced within macrocycles **A-o**, **B-o**, and **C-o**, are shown (derived from **12** by introduction of two cysteines at positions A, B and C, respectively). Heat map depicts ability of resulting compounds to compete with the TCF-4/β-catenin interaction. Data is based on an FP competition assay in analogy to Figure 2b but employing a single competitor concentration ($c = 30$ μM, 0% inhibition = absence of competitor, 100% inhibition = 30 μM **E-CBD** (lower plateau, Figure 2b, Supporting Table S4 and Figure S5)). d) Concentration-dependent inhibition in FP competition assay (Supporting Figure S5) of **A-b5**, **A-b6** and **A-b7** including their monocyclic precursor **A-o** ($c = 7.9\times10^{-3}$–188 μM, $n = 3$, ± std. error). Constant concentration of TCF-4 tracer peptide (10 nM) and β-catenin (250 nM) was employed. e) Concentration-dependent inhibition in FP competition assay (Supporting Figure S5) of **C-b5** and **C-b7** including their monocyclic precursor **C-o** ($c = 7.9\times10^{-3}$–188 μM, $n = 3$, ± std. error). Constant concentration of TCF-4 tracer peptide (10 nM) and β-catenin (250 nM) was employed.

harbors the aromatic *ortho*-xylene moiety (Figure 3c). The monocyclic double-cysteine precursors (**A-o**, **B-o** and **C-o**) were synthesized in analogy to macrocycle **12**, and subsequently reacted with each of the bis-electrophiles (**e1**–**e7**). Conditions for this bicyclization reaction were adjusted to the reactivity of the corresponding bis-electrophile. While **e4**, **e6** and **e7** reacted rapidly in ammonium carbonate buffer and acetonitrile (1:1, v/v), the bicyclization with **e1**, **e2**, **e3** and **e5** was performed in a mixture of water and tetrahydrofuran (1:1, v/v) with large excess of the bis-electrophile (10–50 equiv.) and triethylamine (15–75 equiv.) to ensure sufficient product formation. In addition, the three disulfide-bridged derivatives (**A-ox**, **B-ox** and **C-ox**) were obtained by oxidation. All peptides were purified via HPLC providing product yields between 7% and 64% for the final bicyclization.

The generated 24 bicycles and 3 monocycles were subsequently assessed for their ability to inhibit the TCF-4/β-catenin interaction. Using the FP competition assay described above (Supporting Figure S5), all derivatives were screened at a concentration of 30 μM (Figure 3c, Supporting Table S4). For series A and C, we observed similar trends with low competition capabilities (< 25%) for the monocycles (**A-o**, **C-o**) as well as the bicyclic derivatives with short cross-strand bridges (b1 and b2). For longer bridges, inhibitory potency increased with the highest activities observed for bicycles with four bridging atoms (**A-b5/6/7** and **C-b5/7**). The B-series exhibited overall lower competition without a clear trend regarding changes in the lengths of the cross-strand bridge. Subsequently, the concentration-dependent effect of the most active peptides (inhibition > 50%, **A-b5/6/7** and **C-b5/7**) was investigated (Figure 3d and e). The two monocyclic peptides **A-o** and **C-o** showed considerably lower activity (IC_{50} approx. 100 μM and below) than macrocycle **12** (IC_{50} = 16 μM) indicating that cysteine variation affects β-catenin binding. Notably, the five selected bicycles showed efficient inhibitory activity exceeding that of macrocycle **12**. For the tested A-series bicycles, obtained IC_{50}-values indicated a low dependency on the degree of saturation within the bridge (IC_{50} = 8.5–11 μM for **A-b5/6/7**). From all tested bicycles, *ortho*-xylene bridged **C-b7** exhibited the highest inhibitory activity (IC_{50} = 4.8 μM), which is comparable to the 52-mer peptide **E-CBD** (IC_{50} = 5.4 μM).

Bicyclic β-Sheet Mimetics Inhibit Wnt Signaling

Since some of the library members show inhibition of the TCF-4/β-catenin interaction in biochemical assays, we were interested if this also translates into the inhibition of the Wnt signaling pathway in a cellular context. Therefore, we chose the TOPFLASH reporter gene assay[26] for activity testing which is sensitive to activated Wnt signaling and should respond to the inhibition of the TCF/β-catenin interaction. Briefly, the TOPFLASH reporter plasmid[26] encoding a firefly luciferase gene under control of a TCF/β-catenin-dependent promoter, and a Wnt-independent control reporter plasmid encoding a renilla luciferase were co-transfected into HEK293T cells. The Wnt signaling pathway was activated by incubation with recombinant Wnt-3a protein ligand in the presence of inhibitor (t = 24 h). Wnt-reporter activity was calculated based on the subsequently measured firefly and renilla luciferase signals: firefly/renilla ratios were normalized with respect to the absence and presence of Wnt-3a (0% and 100% rel. reporter activity, respectively). To verify assay functionality, we tested the known upstream Wnt pathway inhibitor XAV939 which promotes β-catenin degradation[27] and indeed shows the expected reduction in reporter activity (30% rel. reporter activity, Figure 4a). Initially, all series A, B and C bicycles with four-atom bridges (b5/6/7) were tested (c = 20 μM, t = 24 h). Notably, the Wnt-independent renilla activity was only mildly affected (Supporting Figure S11) indicating that HEK293T cells tolerate this treatment. Interestingly, macrocycle **12** did not display a meaningful inhibition of Wnt reporter activity, while considerable inhibition was observed for the bicycles of series A (**A-b5/6/7**, Figure 4a). However, none of the series B and C derivatives showed significant reduction of reporter activity (Figure 4a). Among the tested bicycles, the highest inhibitory activity was observed for butene-bridged **A-b6** (43% rel. reporter activity).

Due to its activity in the reporter gene assay, bicycle **A-b6** (Supporting Figure S12) was chosen for follow-up characterization. For comparison, we included monocycle **12** and its linearized analog **12-l**. Initially, a concentration-dependent TOPFLASH reporter gene assay was performed showing robust Wnt inhibition for **A-b6** (IC_{50} = 8 μM, Figure 4b) with high inhibitory activity at 50 μM (2% residual activity). Neither monocycle **12** nor linear analog **12-l** displayed inhibition under these conditions (Figure 4b). Having characterized binding in a competition format (Figure 2b and 3d), we sought to determine dissociation constants (K_d) in a direct FP assay. For that purpose, **12-l** was fluorescently labeled at the N-terminus. Since **12** and **A-b6** do not possess an N-terminus, we substituted a non-interacting amino acid (N631) with a lysine, which was subsequently labeled with an *N*-hydroxysuccinimide ester of fluorescein. FP titration experiments with full-length β-catenin revealed highest affinity for **A-b6** (K_d = 91 nM) followed by monocycle **12** (K_d = 156 nM). The linear analog **12-l** exhibited low affinity (K_d approx. 2 μM). These results follow the trend observed in above FP competition assays: IC_{50} = 8.5 μM (**A-b6**), 16 μM (**12**), > 100 μM (**12-l**). To assess the conformation of these three compounds in solution, circular dichroism (CD) spectra were recorded (Figure 4d). For linear **12-l** (grey), a minimum slightly below λ = 200 nm was observed which is indicative of a dominant random coil character, albeit with some degree of β-sheet formation as a shoulder around λ = 215 nm was observed.[28] In contrast, the spectrum of monocycle **12** (blue) showed a minimum at λ = 215 nm indicating an increase in β-sheet character. Bicycle **A-b6** displayed the strongest β-sheet character as shown by the pronounced minimum at λ = 215 nm and the maximum around λ = 200 nm.[28]

Observed differences in cellular activity (**A-b6** ⩾ **12** ≈ **12-l**) cannot solely be explained with compound affinity for β-catenin (**A-b6** > **12** ⩾ **12-l**). We suspected differences in cellular uptake to be responsible for this discrepancy and therefore assessed their cell penetration properties using again HEK293T cells. Initially, compounds were incubated

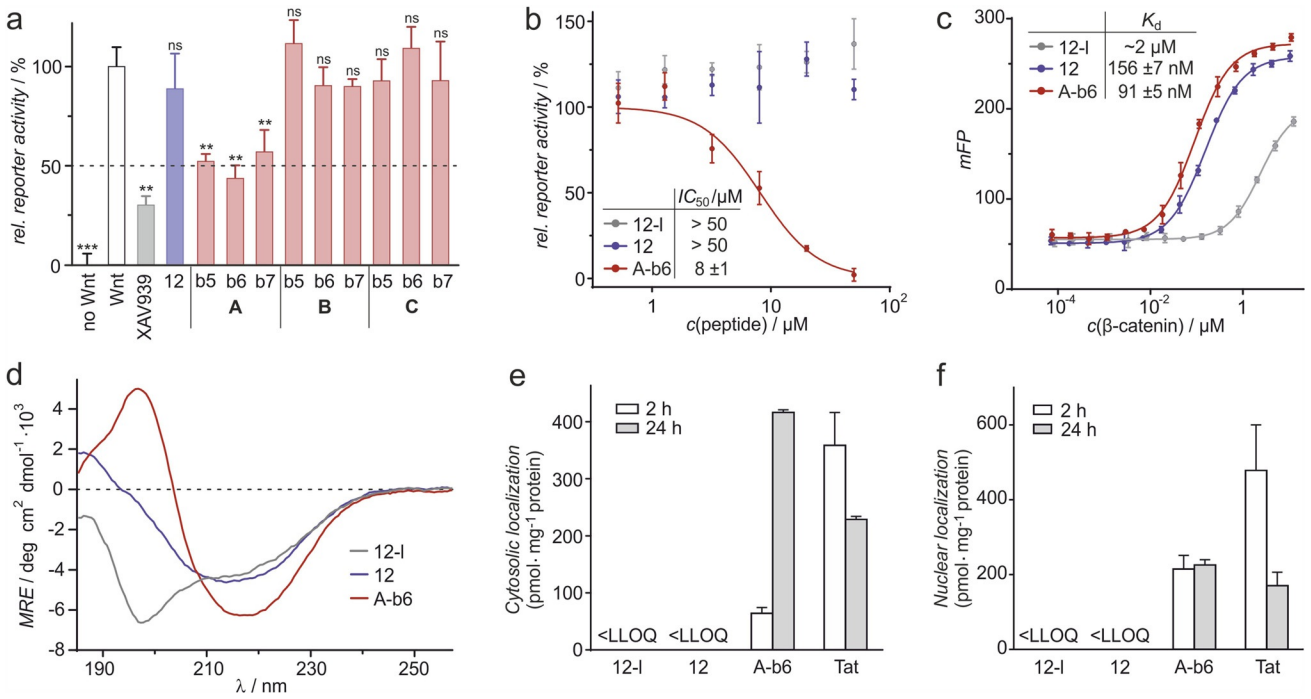

Figure 4. a) TOPFLSH reporter gene assay in HEK293T cells testing inhibition of the Wnt pathway for macrocycle **12** and selected bicycles ($n=3$, error shows std. dev., ns: $p>0.05$, *: $p<0.05$, **: $p<0.01$, ***: $p<0.001$). Wnt signaling was activated with Wnt-3a ($c=100$ ng mL^{-1}). Cells were incubated with compound ($c=20$ µM, $t=24$ h), before luciferase activity was measured (for details see Supporting Methods). b) Concentration-dependent effect on reporter activity for **12-I**, **12** and **A-b6** ($c=0.512$–50 µM, incubation $t=24$ h, $n=3$, ± std. error). c) FP titration measurements of the fluorescein-labeled analogues of **12-I**, **12** and **A-b6** ($c=10$ nM, Supporting Table S1 and S2) and β-catenin (7×10^{-5}–12.6 µM, $n=3$, ± std. error). d) CD spectra of **12-I**, **12** and **A-b6** ($c=75$ µM) in sodium phosphate buffer (5 mM, pH 7.5). e) Cytosolically localized compound ($c=20$ µM) in HEK293T cells after 2 h (white) and 24 h (grey) incubation. Quantification was performed via mass spectrometry using total cytosolic protein as reference ($n=3$, errors show std. dev., LLOQ: lower limit of quantification). f) Compound localized to the nucleus of HEK293T cells after 2 h (white) and 24 h (grey) incubation ($c=20$ µM). Quantification was performed via mass spectrometry using total cytosolic protein as reference ($n=3$, errors show std. dev., LLOQ: lower limit of quantification). **Tat** is a cell-permeable peptide (for sequence see Supporting Table S1).

($t=24$ h) in cell culture media including 10% fetal bovine serum (FBS) and in presence of HEK293T cells. Mass spectrometry (MS) measurements confirmed the presence of all three peptides after 24 h (Supporting Figure S13). However, while **A-b6** and **12** provided signals in the range of the starting point, **12-I** showed considerably reduced signal intensity (ca. 50%) presumably due to proteolytic degradation. To assess the cell penetration properties, cytoplasmic and nuclear localization was determined after sub-cellular fractionation using a MS-based methodology.[29] In these experiments, we included cell-penetrating peptide **Tat** as reference. HEK293T cells were incubated with compounds ($c=20$ µM) for 2 or 24 h, then the cells were lysed and fractionated to isolate cytoplasmic and nuclear contents for subsequent LC-MS analysis (Supporting Figures S14–S18, Table S5–S8). While we did not observe cytosolic localization for linear **12-I** and monocyclic **12**, bicycle **A-b6** showed time-dependent cytosolic accumulation (Figure 4e), which after 24 h exceeds cell-penetrating peptide **Tat**. We also observed nuclear uptake of **A-b6** and **Tat**, which was not the case for **12** and **12-I** (Figure 4f). Here, it is important to note, that subcellular concentrations are reported relative to the corresponding total protein concentrations and cannot be directly compared between different cellular compartments.

Conclusion

Due to its involvement in the onset and progression of numerous types of cancers, hyperactive Wnt signaling has moved into the focus of drug discovery efforts. In an oncogenic context, Wnt signaling is often activated via mutations in central pathway regulators. For that reason, targeting the downstream β-catenin/TCF transcriptional activator complex has been pursued. TCF transcription factors recognize the armadillo repeat domain of β-catenin via an elongated peptide sequence (green, Figure 1a) with two central hot spot residues crucially contributing to binding. Previous structure-based efforts to generate ligands targeting the corresponding site on β-catenin (binding site 3)[20e,30] have not resulted in therapeutically useful inhibitors. Herein, we took a novel approach towards the generation of ligands for β-catenin's binding site 3 using E-cadherin as a starting point. We noticed that the CBD of E-cadherin binds to site 3 via an antiparallel β-sheet which may serve as the basis for inhibitor design. However, while the 52-mer E-cadherin epitope (**E-CBD**) showed high affinity for β-catenin ($K_d=53$ nM), we were unable to identify a considerably truncated version with sufficient affinity (e.g. 14-mer **11**, $K_d>5$ µM). Most notably, macrocyclization of 14-mer peptide **11** using the DP-LP turn

motif resulted in a molecule with greatly improved affinity (**12**, $K_d = 156$ nM).

We were able to co-crystalize macrocycle **12** with β-catenin providing a crystal structure that confirms the expected binding site 3 and an antiparallel β-sheet arrangement of **12**. This is the first crystal structure of a synthetic ligand bound to this site of β-catenin. In fact, only two crystal structures of synthetic ligands bound to β-catenin had been reported so far.[20f,31] Based on the structure of **12** bound to β-catenin, a focused library of bicyclic inhibitors was synthesized applying a late-stage diversification strategy. The library was obtained by reacting unprotected monocyclic peptides bearing two cross-strand cysteines with seven different bis-electrophiles. Three distinct monocyclic precursors were used providing a total of 21 thioether bridged bicycles. A competition assay using β-catenin and the CBD of TCF-4 as tracer, revealed diminished inhibitory activity for macrocyclic double-cysteine variants while the installation of four-carbon atom bridges restored inhibitory activity for two of the three scaffolds (**A-b5/6/7** and **C-b5/7**). Best performing library members showed affinities in the range of the 52-mer starting sequence (**E-CBD**) which highlights the impact of conformational constrain on binding.

In a Wnt reporter gene assay, only series A peptides (**A-b5/6/7**) showed inhibitory activity with **A-b6**, encompassing a butene bridge, performing best ($IC_{50} = 8$ μM). In contrast, monocyclic precursor **12** did not show cellular activity (highest tested concentration 50 μM). This is a surprising finding which cannot solely be explained by differences in competition with TCF: $IC_{50} = 16$ μM (**12**) vs. 8.5 μM (**A-b6**). CD analysis showed that bicycle **A-b6** exhibits a more pronounced β-hairpin structure than monocyclic peptide **12**. This was accompanied by robust cellular uptake in the range of cell-penetrating peptide **Tat**. Thus, the more pronounced β-sheet character of free bicycle **A-b6** may contribute to cell penetration. Taken together, β-sheet mimetic **A-b6** represents an appealing starting point for the development of potentially useful anti-cancer agents targeting the TCF/β-catenin interaction. Moreover, the presented design strategy towards bicyclic peptides is a rare example of a structure-based development of cell-permeable β-sheet mimetics, and it can serve as a basis for the development of novel inhibitors for other β-sheet-mediated protein–protein interactions.

Acknowledgements

This work was supported by the European Research Council (ERC starting grant number 678623). R.B. was supported by UniNA and Compagnia di San Paolo, in the frame of Programme STAR 2018. We thank the I04 beamline staff of the Diamond Light Source (UK) for support.

Conflict of interest

MW, RB, AG, N-LE, TvR and TNG are listed as inventors on a patent application related to described peptidomimetics.

Keywords: cell-penetrating peptides · macrocycles · peptidomimetics · protein–protein interactions · thioether crosslinks

[1] a) W. S. Horne, T. N. Grossmann, *Nat. Chem.* **2020**, *12*, 331 – 337; b) L.-G. Milroy, T. N. Grossmann, S. Hennig, L. Brunsveld, C. Ottmann, *Chem. Rev.* **2014**, *114*, 4695 – 4748.

[2] a) M. Pelay-Gimeno, A. Glas, O. Koch, T. N. Grossmann, *Angew. Chem. Int. Ed.* **2015**, *54*, 8896 – 8927; *Angew. Chem.* **2015**, *127*, 9022 – 9054; b) A. D. Cunningham, N. Qvit, D. Mochly-Rosen, *Curr. Opin. Struct. Biol.* **2017**, *44*, 59 – 66.

[3] a) V. Azzarito, K. Long, N. S. Murphy, A. J. Wilson, *Nat. Chem.* **2013**, *5*, 161 – 173; b) P. M. Cromm, J. Spiegel, T. N. Grossmann, *ACS Chem. Biol.* **2015**, *10*, 1362 – 1375; c) J. Iegre, J. S. Gaynord, N. S. Robertson, H. F. Sore, M. Hyvönen, D. R. Spring, *Adv. Ther.* **2018**, *1*, 1800052; d) D. A. Guarracino, J. A. Riordan, G. M. Barreto, A. L. Oldfield, C. M. Kouba, D. Agrinsoni, *Chem. Rev.* **2019**, *119*, 9915 – 9949.

[4] A. M. Watkins, P. S. Arora, *ACS Chem. Biol.* **2014**, *9*, 1747 – 1754.

[5] a) J. Laxio Arenas, J. Kaffy, S. Ongeri, *Curr. Opin. Chem. Biol.* **2019**, *52*, 157 – 167; b) H. I. Merritt, N. Sawyer, P. S. Arora, *Pept. Sci.* **2020**, *112*, e24145.

[6] J. A. Robinson, *Chimia* **2013**, *67*, 885 – 890.

[7] P.-N. Cheng, C. Liu, M. Zhao, D. Eisenberg, J. S. Nowick, *Nat. Chem.* **2012**, *4*, 927 – 933.

[8] a) C. K. Wang, D. J. Craik, *Nat. Chem. Biol.* **2018**, *14*, 417 – 427; b) B. L. Kier, J. M. Anderson, N. H. Andersen, *J. Am. Chem. Soc.* **2015**, *137*, 5363 – 5371; c) A. M. Almeida, R. Li, S. H. Gellman, *J. Am. Chem. Soc.* **2012**, *134*, 75 – 78.

[9] a) A. M. White, S. J. de Veer, G. Wu, P. J. Harvey, K. Yap, G. J. King, J. E. Swedberg, C. K. Wang, R. H. P. Law, T. Durek, D. J. Craik, *Angew. Chem. Int. Ed.* **2020**, *59*, 11273 – 11277; *Angew. Chem.* **2020**, *132*, 11369 – 11373; b) V. Celentano, D. Diana, C. Di Salvo, L. de Rosa, A. Romanelli, R. Fattorusso, L. D. D'Andrea, *Chem. Eur. J.* **2016**, *22*, 5534 – 5537; c) L. E. Hanold, K. Oruganty, N. T. Ton, A. M. Beedle, N. Kannan, E. J. Kennedy, *PLoS One* **2015**, *10*, e0118796; d) J. H. Park, M. L. Waters, *Org. Biomol. Chem.* **2013**, *11*, 69 – 77; e) M. Empting, O. Avrutina, R. Meusinger, S. Fabritz, M. Reinwarth, M. Biesalski, S. Voigt, G. Buntkowsky, H. Kolmar, *Angew. Chem. Int. Ed.* **2011**, *50*, 5207 – 5211; *Angew. Chem.* **2011**, *123*, 5313 – 5317; f) K. Holland-Nell, M. Meldal, *Angew. Chem. Int. Ed.* **2011**, *50*, 5204 – 5206; *Angew. Chem.* **2011**, *123*, 5310 – 5312.

[10] a) M. I. García-Aranda, Y. Mirassou, B. Gautier, M. Martín-Martínez, N. Inguimbert, M. Vidal, M. T. García-López, M. A. Jiménez, R. González-Muñiz, M. J. Pérez de Vega, *Bioorg. Med. Chem.* **2011**, *19*, 7526 – 7533; b) S. Giddu, V. Subramanian, H. S. Yoon, S. D. Satyanarayanajois, *J. Med. Chem.* **2009**, *52*, 726 – 736; c) D. Yang, W. Qin, X. Shi, B. Zhu, M. Xie, H. Zhao, B. Teng, Y. Wu, R. Zhao, F. Yin, P. Ren, L. Liu, Z. Li, *J. Med. Chem.* **2018**, *61*, 8174 – 8185.

[11] a) B. Zhao, D. Yang, J. H. Wong, J. Wang, C. Yin, Y. Zhu, S. Fan, T. B. Ng, J. Xia, Z. Li, *ChemBioChem* **2016**, *17*, 1416 – 1420; b) H.-K. Cui, Y. Guo, Y. He, F.-L. Wang, H.-N. Chang, Y.-J. Wang, F.-M. Wu, C.-L. Tian, L. Liu, *Angew. Chem. Int. Ed.* **2013**, *52*, 9558 – 9562; *Angew. Chem.* **2013**, *125*, 9737 – 9741.

[12] H. Lingard, J. T. Han, A. L. Thompson, I. K. H. Leung, R. T. W. Scott, S. Thompson, A. D. Hamilton, *Angew. Chem. Int. Ed.* **2014**, *53*, 3650 – 3653; *Angew. Chem.* **2014**, *126*, 3724 – 3727.

[13] a) M. Vidal, M. E. Cusick, A.-L. Barabási, *Cell* **2011**, *144*, 986 – 998; b) E. Valeur, S. M. Guéret, H. Adihou, R. Gopalakrishnan, M. Lemurell, H. Waldmann, T. N. Grossmann, A. T. Plowright, *Angew. Chem. Int. Ed.* **2017**, *56*, 10294 – 10323; *Angew. Chem.* **2017**, *129*, 10428 – 10459.

[14] O. Keskin, A. Gursoy, B. Ma, R. Nussinov, *Chem. Rev.* **2008**, *108*, 1225 – 1244.

[15] D. E. Scott, A. R. Bayly, C. Abell, J. Skidmore, *Nat. Rev. Drug. Discov.* **2016**, *15*, 533 – 550.
[16] H. Clevers, R. Nusse, *Cell* **2012**, *149*, 1192 – 1205.
[17] K. M. Cadigan, M. L. Waterman, *Cold Spring Harbor Perspect. Biol.* **2012**, *4*, a007906.
[18] C. Cui, X. Zhou, W. Zhang, Y. Qu, X. Ke, *Trends Biochem. Sci.* **2018**, *43*, 623 – 634.
[19] a) G. Hahne, T. N. Grossmann, *Bioorg. Med. Chem.* **2013**, *21*, 4020 – 4026; b) X. Zhang, L. Wang, Y. Qu, *Pharmacol. Res.* **2020**, *160*, 104794.
[20] a) Z. Huang, M. Zhang, S. D. Burton, L. N. Katsakhyan, H. Ji, *ACS Chem. Biol.* **2014**, *9*, 193 – 201; b) L. Dietrich, B. Rathmer, K. Ewan, T. Bange, S. Heinrichs, T. C. Dale, D. Schade, T. N. Grossmann, *Cell Chem. Biol.* **2017**, *24*, 958 – 968; c) P. Diderich, D. Bertoldo, P. Dessen, M. M. Khan, I. Pizzitola, W. Held, J. Huelsken, C. Heinis, *ACS Chem. Biol.* **2016**, *11*, 1422 – 1427; d) T.-H. Hsieh, C.-Y. Hsu, C.-F. Tsai, C.-C. Chiu, S.-S. Liang, T.-N. Wang, P.-L. Kuo, C.-Y. Long, E.-M. Tsai, *Sci. Rep.* **2016**, *6*, 19156; e) J. A. Schneider, T. W. Craven, A. C. Kasper, C. Yun, M. Haugbro, E. M. Briggs, V. Svetlov, E. Nudler, H. Knaut, R. Bonneau, M. J. Garabedian, K. Kirshenbaum, S. K. Logan, *Nat. Commun.* **2018**, *9*, 4396; f) T. N. Grossmann, J. T.-H. Yeh, B. R. Bowman, Q. Chu, R. E. Moellering, G. L. Verdine, *Proc. Natl. Acad. Sci. USA* **2012**, *109*, 17942 – 17947; g) B. Yu, Z. Huang, M. Zhang, D. R. Dillard, H. Ji, *ACS Chem. Biol.* **2013**, *8*, 524 – 529.
[21] a) F. Poy, M. Lepourcelet, R. A. Shivdasani, M. J. Eck, *Nat. Struct. Biol.* **2001**, *8*, 1053 – 1057; b) T. A. Graham, D. M. Ferkey, F. Mao, D. Kimelman, W. Xu, *Nat. Struct. Biol.* **2001**, *8*, 1048 – 1052; c) J. Sampietro, C. L. Dahlberg, U. S. Cho, T. R. Hinds, D. Kimelman, W. Xu, *Mol. Cell* **2006**, *24*, 293 – 300.
[22] S. Knapp, M. Zamai, D. Volpi, V. Nardese, N. Avanzi, J. Breton, S. Plyte, M. Flocco, M. Marconi, A. Isacchi, V. R. Caiolfa, *J. Mol. Biol.* **2001**, *306*, 1179 – 1189.
[23] D. M. Krüger, H. Gohlke, *Nucleic Acids Res.* **2010**, *38*, W480 – W486.
[24] a) C. M. Nair, M. Vijayan, Y. V. Venkatachalapathi, P. Balaram, *J. Chem. Soc. Chem. Commun.* **1979**, 1183 – 1184; b) J. Späth, F. Stuart, L. Jiang, J. A. Robinson, *Helv. Chim. Acta* **1998**, *81*, 1726 – 1738.
[25] a) H. Jo, N. Meinhardt, Y. Wu, S. Kulkarni, X. Hu, K. E. Low, P. L. Davies, W. F. DeGrado, D. C. Greenbaum, *J. Am. Chem. Soc.* **2012**, *134*, 17704 – 17713; b) P. Timmerman, J. Beld, W. C. Puijk, R. H. Meloen, *ChemBioChem* **2005**, *6*, 821 – 824; c) R. Kowalczyk, P. W. R. Harris, M. A. Brimble, K. E. Callon, M. Watson, J. Cornish, *Bioorg. Med. Chem.* **2012**, *20*, 2661 – 2668; d) D. P. Fairlie, A. Dantas de Araujo, *Biopolymers* **2016**, *106*, 843 – 852; e) C. Heinis, T. Rutherford, S. Freund, G. Winter, *Nat. Chem. Biol.* **2009**, *5*, 502 – 507.
[26] a) V. Korinek, N. Barker, P. J. Morin, D. van Wichen, R. de Weger, K. W. Kinzler, B. Vogelstein, H. Clevers, *Science* **1997**, *275*, 1784 – 1787; b) M. T. Veeman, D. C. Slusarski, A. Kaykas, S. H. Louie, R. T. Moon, *Curr. Biol.* **2003**, *13*, 680 – 685.
[27] T. Sakata, J. K. Chen, *Chem. Soc. Rev.* **2011**, *40*, 4318 – 4331.
[28] N. J. Greenfield, *Nat. Protoc.* **2006**, *1*, 2876 – 2890.
[29] a) W. McCoull, T. Cheung, E. Anderson, P. Barton, J. Burgess, K. Byth, Q. Cao, M. P. Castaldi, H. Chen, E. Chiarparin, R. J. Carbajo, E. Code, S. Cowan, P. R. Davey, A. D. Ferguson, S. Fillery, N. O. Fuller, N. Gao, D. Hargreaves, M. R. Howard, J. Hu, A. Kawatkar, P. D. Kemmitt, E. Leo, D. M. Molina, N. O'Connell, P. Petteruti, T. Rasmusson, P. Raubo, P. B. Rawlins, P. Ricchiuto, G. R. Robb, M. Schenone, M. J. Waring, M. Zinda, S. Fawell, D. M. Wilson, *ACS Chem. Biol.* **2018**, *13*, 3131 – 3141; b) P. M. Cromm, H. Adihou, S. Kapoor, M. Vazquez-Chantada, P. Davey, D. Longmire, E. Hennes, W. Hofer, P. Küchler, E. Chiarparin, H. Waldmann, T. N. Grossmann, *ChemBioChem* **2019**, *20*, 2987 – 2990; c) H. Adihou, R. Gopalakrishnan, T. Förster, S. M. Guéret, R. Gasper, S. Geschwindner, C. Carrillo García, H. Karatas, A. V. Pobbati, M. Vazquez-Chantada, P. Davey, C. M. Wassvik, J. K. S. Pang, B. S. Soh, W. Hong, E. Chiarparin, D. Schade, A. T. Plowright, E. Valeur, M. Lemurell, T. N. Grossmann, H. Waldmann, *Nat. Commun.* **2020**, *11*, 5425.
[30] Z. Wang, M. Zhang, J. Wang, H. Ji, *J. Med. Chem.* **2019**, *62*, 3617 – 3635.
[31] D. Kessler, M. Mayer, S. K. Zahn, M. Zeeb, S. Wöhrle, A. Bergner, J. Bruchhaus, T. Ciftci, G. Dahmann, M. Dettling, S. Döbel, J. E. Fuchs, L. Geist, W. Hela, C. Kofink, R. Kousek, F. Moser, T. Puchner, K. Rumpel, M. Scharnweber, P. Werni, B. Wolkerstorfer, D. Breitsprecher, P. Baaske, M. Pearson, D. B. McConnell, J. Böttcher, *ChemMedChem* **2021**, https://doi.org/10.1002/cmdc.202000839.

Manuscript received: February 9, 2021
Accepted manuscript online: March 29, 2021
Version of record online: May 5, 2021

